(2)

OFFICE OF NAVAL RESEARCH

Grant N00014-91-J-1550

R&T Code: 413w003

Technical Report No. 4

Atomic force microscopy of (100), (110), and (111) homoepitaxial diamond films

by

L. F. Sutcu, C. J. Chu, M. S. Thompson, R. H. Hauge, J. L. Margrave, and M. P. D'Evelyn

Published in

Journal of Applied Physics **71**, 5930 (1992)

Rice University
Department of Chemistry
Houston, TX 77251-1892

May 29, 1992

REPORT DOCUMENTATION PAGE

Form Approved
OMB No. 0704-0188

1. AGENCY USE ONLY (Leave blank)	2. REPORT DATE	3. REPORT TYPE AND DATES COVERED
	May 1992	Technical

4. TITLE AND SUBTITLE
Atomic force microscopy of (100), (110), and (111) homoepitaxial diamond films

5. FUNDING NUMBERS
Grant #:
N00014-91-J-1550

6. AUTHOR(S)
L. F. Sutcu, C. J. Chu, M. S. Thompson, R. H. Hauge, J. L. Margrave, and M. P. D'Evelyn

7. PERFORMING ORGANIZATION NAME(S) AND ADDRESS(ES)
Rice University
Department of Chemistry
Houston, TX 77251-1892

8. PERFORMING ORGANIZATION REPORT NUMBER
Technical Report
#4

9. SPONSORING/MONITORING AGENCY NAME(S) AND ADDRESS(ES)
Office of Naval Research
800 N. Quincy Street
Arlington, VA 22217-5000

10. SPONSORING/MONITORING AGENCY REPORT NUMBER

11. SUPPLEMENTARY NOTES
Published in:
Journal of Applied Physics **71**, 5930-5940 (1992).

12a. DISTRIBUTION/AVAILABILITY STATEMENT
Approved for public release; distribution is unlimited.

12b. DISTRIBUTION CODE

13. ABSTRACT *(Maximum 200 words)*

We present atomic force microscopy images of diamond films grown by chemical vapor deposition epitaxially on diamond (100), (110), and (111) substrates. The films were grown from 0.2-1.6% mixtures of CH_4 and C_2H_2 in H_2 in a hot-filament reactor at a total pressure of 25 Torr. The substrate and filament temperatures were held at 810-1000 °C and 2000-2150 °C, respectively. A (100)-oriented diamond film grown with 0.3% CH_4 at a substrate temperature of 810 °C was rough on the μm scale, exhibiting pyramidal features, terraces, and penetration twins, while films grown at higher substrate temperatures and hydrocarbon flow rates were smooth on the nm scale and showed evidence of a (2×1) reconstruction. A (110)-oriented film was very rough on the μm scale but nearly atomically smooth on the 0.5-5 nm scale and exhibited local slopes higher than 40° with no evidence of faceting. A film grown on a diamond (111) substrate underwent spontaneous fracture due to tensile stress and exhibited a roughness of ≈10-50 nm on the ≈100 nm lateral scale in regions far away from any cracks. The implications of the morphological features for diamond growth mechanisms are discussed.

14. SUBJECT TERMS
Diamond, chemical vapor deposition, homoepitaxy, atomic force microscopy

15. NUMBER OF PAGES

16. PRICE CODE

17. SECURITY CLASSIFICATION OF REPORT	18. SECURITY CLASSIFICATION OF THIS PAGE	19. SECURITY CLASSIFICATION OF ABSTRACT	20. LIMITATION OF ABSTRACT
Unclassified	Unclassified	Unclassified	

Atomic force microscopy of (100), (110), and (111) homoepitaxial diamond films

L. F. Sutcu, C. J. Chu,* M. S. Thompson,** R. H. Hauge,* J. L. Margrave,* and M. P. D'Evelyn

Department of Chemistry and Rice Quantum Institute, Rice University, Houston, TX 77251-1892

*Also affiliated with *Houston Advanced Research Center, 4802 Research Forest Dr., The Woodlands, TX 77381*

**Digital Instruments, Inc., 6780 Cortona Drive, Santa Barbara, CA 93117*

Abstract

We present atomic force microscopy images of diamond films grown by chemical vapor deposition epitaxially on diamond (100), (110), and (111) substrates. The films were grown from 0.2-1.6% mixtures of CH_4 and C_2H_2 in H_2 in a hot-filament reactor at a total pressure of 25 Torr. The substrate and filament temperatures were held at 810-1000 °C and 2000-2150 °C, respectively. A (100)-oriented diamond film grown with 0.3% CH_4 at a substrate temperature of 810 °C was rough on the μm scale, exhibiting pyramidal features, terraces, and penetration twins, while films grown at higher substrate temperatures and hydrocarbon flow rates were smooth on the nm scale and showed evidence of a (2×1) reconstruction. A (110)-oriented film was very rough on the μm scale but nearly atomically smooth on the 0.5-5 nm scale and exhibited local slopes higher than 40° with no evidence of faceting. A film grown on a diamond (111) substrate underwent spontaneous fracture due to tensile stress and exhibited a roughness of ≈10-50 nm on the ≈100 nm lateral scale in regions far away from any cracks. The implications of the morphological features for diamond growth mechanisms are discussed.

Journal of Applied Physics (in press)

I. INTRODUCTION

The extreme properties of diamond and myriad of applications for diamond thin films have motivated the rapid growth of chemical vapor deposition (CVD) growth technology. For electronic applications in particular there is great interest in growth of high quality single crystal diamond films, and diamond homoepitaxy has been achieved by many research groups.[1-11] Homoepitaxial growth studies also promise to be extremely useful in advancing our level of understanding of the growth mechanism(s). Although much has been learned about the gas-phase chemistry in hot-filament CVD environments[12-14] and several detailed models of diamond growth have been proposed,[15-20] virtually nothing is known about the details of the decomposition of CH_x intermediates on the growing surface. Characterization of film morphologies on the near-atomic scale may help elucidate some of these growth details, and may be useful as well in better understanding nucleation and the factors that control morphology on the micron scale.

Electron microscopy has been by far the dominant tool for morphological characterization of diamond films. However, scanning tunneling microscopy (STM) and atomic force microscopy (AFM) routinely achieve atomic resolution on many substrates, and seem much better suited to determination of the nanometer-scale structure of diamond films. Several groups have applied STM to characterization of B-doped and undoped polycrystalline diamond films,[21-25] but only a limited resolution has been achieved to date. Near atomic-level resolution has recently been achieved by Tsuno *et al.* by STM on a homoepitaxial (100) diamond film.[26] The need for electrically-conducting substrates for STM appears to be a serious limitation for characterization of diamond films, and AFM, which has no such requirement, would seem to be a more generally applicable tool. The ability to characterize undoped films is particularly important because boron doping has been shown to change the surface morphology of diamond films.[4,25] However, early AFM images of polycrystalline diamond films[25,27] have been limited to a resolution of $\approx$ 30 nm.

In this study we have examined the surface topography of homoepitaxial diamond films grown by hot-filament CVD on (100)-, (110)-, and (111)-oriented natural diamond single-crystal substrates by AFM. A preliminary account of this work has been reported previously.[28]

II. EXPERIMENTAL

Homoepitaxial diamond films were grown by hot-filament CVD in a reactor that has been described in detail previously.[9,13a] The filaments consisted of six strands of 0.13-mm-diameter tungsten wire approximately 10 mm in length which were resistively heated. The single-crystal, type 2A natural diamond substrates, obtained from Dubbeldee Harris, were 1.5×1.5 mm^2 in area and 0.1 mm thick, and were placed in a foil heater situated $\approx$9 mm below the filament after rinsing

with acetone. The temperatures of the filament and samples were measured by an optical pyrometer and a Pt/Pt-13%Rh thermocouple, respectively. The total pressure in the reactor was held at 25 torr during each deposition. A total of five films were analyzed in this study; the experimental growth conditions used for each sample are tabulated in Table I. Hydrogen was introduced above the filament and hydrocarbon gas(es) were injected between the filament and sample during growth of samples I-IV, as described previously.[9,13a] Both the hydrogen and hydrocarbon were introduced above the filament during growth of sample V. A mixture of $^{13}CH_4$ and $^{12}C_2H_2$ was used in growing samples II and IV, while unlabeled methane was used for samples I, III, and V. Sample V, with a total film thickness of 9.2 μm,was used in a study of homoepitaxial growth kinetics, as reported elsewhere.[29] The CH_4 flow rate was varied from 0.3 to 1.3 sccm, corresponding to hydrocarbon mole fractions of 0.2-0.85%. The final growth step for sample V employed 0.6 sccm (0.3%) CH_4 and yielded a 1.0-μm-thick film.

AFM images were obtained in ambient air using a Digital Instruments Nanoscope II AFM utilizing an optical lever in combination with a microfabricated Si_3N_4 tip and cantilever. The AFM was operated in the repulsive force mode. Typical forces between the sample and the tip were in the range of 10^{-6}-10^{-8} N. Most AFM images of samples were acquired within a few weeks after their growth. Several samples were later re-scanned by AFM (images not shown) following treatment in boiling, concentrated sulfuric acid to remove graphite and other impurities. The appearance of surface features was very similar, as discussed below, but the amount of unidentified debris increased slightly.

The samples were also characterized by Raman spectroscopy, using a Spex Raman spectrometer and 514 nm (2.41 eV) Ar^+ laser excitation.

III. RESULTS

Raman spectra of samples I-IV are shown in Fig. 1. The Raman spectrum of sample I, shown in Fig. 1(a), shows the sharp first-order Raman peak of diamond at 1332 cm^{-1} and no evidence of a graphitic feature near 1550 cm^{-1}.[30-32] The signal intensity in this spectrum was lower than that in spectra obtained from other samples, presumably due to scattering caused by the roughness of the surface, and the amplitude has been multiplied by 10 in order to better show the baseline. The 1332 cm^{-1} peak in Fig. 1(a) contains contributions from both the substrate and the film, based on a comparison with micro-Raman spectra (not shown). Micro-Raman spectra obtained from different regions of sample I were nearly identical and very similar to Fig. 1(a), albeit with a smaller 1332 cm^{-1} peak. The shoulder on the high-frequency side of the 1332 cm^{-1} peak has been observed previously in polycrystalline diamond films[32] and may be due to defects, but is probably not due to

amorphous or graphitic carbon since it should have been accompanied by a more intense peak near 1550 cm^{-1}.[30-32]

The Raman spectra of samples II, III, and IV, shown in Fig. 1(b), (c), and (d), respectively, similarly show no evidence of graphitic carbon, and also no indication of a high-frequency shoulder on the 1332 cm^{-1} peak. As samples II and IV comprise 57%-^{13}C/33%-^{12}C films,[13b] the Raman fundamental of the diamond film occurs at 1308 cm^{-1} and is distinct from the peak due to the substrate. Unfortunately, sample V was lost after acquisition of the AFM images and we were unable to obtain its Raman spectrum. However, all homoepitaxial (111) diamond films that we have grown have a small-amplitude, broad Raman peak near 1550 cm^{-1}, indicating graphitic inclusions, as reported previously,[9] and this was presumably also true for sample V.

A large area (0.1×0.1 mm^2) AFM image of sample I is shown in Fig. 2. The film surface is very rough and faceted, comprising square pyramidal features and sharper triangular features with a total height variation of ≈ 0.8 μm. Both the pyramidal and triangular features follow the square orientation of the (100) substrate, with the triangular features being rotated by ±90° or 180° at random about a principal axis direction. The larger pyramidal features are observable with an optical microscope, proving that the morphology observed by AFM is not an artifact resulting from tip effects. The pyramids are typically 5000-7000 nm wide and 200-300 nm high. Micro-Raman spectra obtained from the pyramids, triangular features and areas in between the pyramids were nearly identical and very similar to Fig. 1(a), indicating that all of the features are high-quality diamond. A higher-resolution image of a portion of sample I is shown in Fig. 3. Some of the pyramids on sample I have smooth sides, while those visible in Fig. 3 show a clear terraced structure with ledges. Some pyramids have ledges 500-1500 nm wide. On some of the pyramids the sloped sides extend up to the top, whereas other pyramids have flat tops, with widths of 500–2000 nm. Typical slopes of the sides of the pyramids and of the regions between ledges are $\approx 5°$ (the vertical scale in Fig. 3 is expanded). Assuming that steps are one atom high (1/4 lattice constant), the 5° slope implies a (100) terrace width of ≈ 10 Å. Sample I was re-scanned by AFM after being boiled overnight in concentrated sulfuric acid, but no changes in the surface features and roughness were observed by AFM after the procedure. We were unable to achieve near-atomic-level resolution on this sample, but with the exception of the tops of the triangular features, the film (near-(100) orientation) was *locally* very smooth, with a roughness on the 1-100 nm scale less than 5 nm in amplitude.

The sharp triangular features seen in Figs. 2 and 3 (which appear dark in Fig. 3) are much rougher than the pyramids in appearance, are typically 400-1000 nm wide and 100-300 nm high, and are identified as penetration twins.[33] They appear to be more or less randomly distributed with respect to the pyramids. Figure 4 shows an isolated penetration twin, also on sample I. The

penetration twins typically have one rough, gently-sloping face and two steeper, smooth faces exposed. The rough faces are almost certainly of <111> orientation, as their morphology is qualitatively identical to that we observe in (111) homoepitaxial films but quite different from that of (100)-oriented films, and only (111) and (100) facets are normally observed in polycrystalline diamond films. The assignment of the triangular features as penetration twins follows from the angle between the normal to the rough face and <100> (the substrate normal), typically 15-20°. This value is much smaller than the angle between <111> and <100> within bulk diamond, 54.7°, which implies the existence of subsurface twin planes beneath the triangular features. The steep sides of the penetration twins make a much sharper angle with respect to the substrate, ≈40-50°. This latter value may underestimate the true angle as the AFM image is essentially a convolution of the shapes of the sample and tip and we do not known precisely how sharp the AFM tip was. The smoothness of the steep sides of the penetration twins suggests that they are of (100) orientation. Nearly identical features were observed on (100) faces of cubo-octahedral diamond crystals by Clausing *et al.*,[34] who similarly identified the rough surface of the penetration twin as being (111)-oriented and the smoother sides as (100) facets. The angle made by the intersection of the two steep sides with the rough face is ≈30°. This value is much smaller than the ideal value of 60° for the intersection of (111) planes with (100) and (010) planes, which in turn implies the existence of a vertically-oriented twin plane in the middle of the triangular features in addition to the subsurface twin.

Fig. 5 shows an AFM line plot of sample II, which was grown at a slightly higher temperature than sample I. The surface is seen to be fairly smooth, with the height varying by 2-4 nm on a lateral length scale of 50-100 nm. Larger-scale scans (not shown) show the same behavior: the amplitude of roughness is only on the order of several nm, in contrast to sample I. The root-mean-square slope is estimated to be 5-10°, implying (100) terrace widths in the range of 5-10 Å, assuming monatomic steps. The morphology is actually very similar to regions on sample I *between* pyramids, which are more widely separated near the edges of the sample than in the regions shown in Figs. 2 and 3. The main change between samples I and II, therefore, is suppression of pyramid and penetration twin formation. AFM scans of an as-polished (111) substrate revealed ridges and scratches from the polishing, with most in the range of 5-10 nm in height and a total height variation of less than 100 nm. The size of preexisting features on the (100) substrate used to grow sample II were presumably similar in size. As the film thickness on sample II (2 μm) is much greater than the probable size of preexisting features, the morphology shown in Fig. 4 is probably intrinsic to the growth conditions, but a possible role of the step density and roughness of the substrate cannot be excluded.

A large-scale three-dimensional image of Sample III is shown in Fig. 6. The surface is

decorated by bumps, ≈ 50-100 nm wide by 1-5 nm high (note the very different vertical and horizontal scales in Fig. 6). We cannot definitively identify the bumps, but we believe them to be adsorbed microdroplets of some kind, as they disappeared after boiling sample III in sulfuric acid. Apart from the bumps, the surface is *extremely* flat–large area AFM scans showed a total height variation of only 1-2 nm over lateral distances of 1000-3000 nm. The root-mean-square slope is in the range of 0.1°, corresponding to (100) terrace widths of ≈ 20 nm, again assuming monatomic steps. Transmission Fourier-transform infrared spectra, used to determine the film thicknesses,[9] provided further evidence of the extreme flatness of the film surface. The amplitude of the interference fringes normally decreases at shorter wavelengths,[9] which we attribute to increased nonspecular scattering as the wavelength of the light approaches the lateral length scale of the surface roughness. After growth of the film on sample III, the intensity of the interference fringes was constant, within experimental error, over the entire 400-4000 cm^{-1} frequency range.

A high-resolution image (5×5 nm^2) of a portion of sample III is shown in Fig. 7. Although individual atoms cannot be seen, evidence is seen for parallel lines separated by 5.00-5.08 Å, as indicated by the white traces added to the upper portion of the figure. We believe that these sets of lines correspond to rows of dimerized surface carbon atoms which would have a theoretical separation of 5.04 Å, corresponding to a (2×1) reconstruction. Cross-sections of the AFM image show that the uppermost rows are ≈ 0.9 Å higher than the rows rotated by 90° below and to the right, corresponding to a type A monatomic step.[35] Similar (2×1) dimer rows and steps have been observed by STM on Si(100)[36,37] and Ge(100)[38] surfaces and, very recently, on a homoepitaxial (100) diamond film.[26] It is not clear why dimer rows cannot be seen in the rest of the image, but cross-sectional height measurements suggest that the upper and left-hand part of the image constitute the upper terrace and the remainder comprises the lower terrace. The structural model we propose for the AFM image shown in Fig. 7 is shown in Fig. 8. The shift in the rows on the upper terrace evident in Figs. 7 and 8 is an antiphase domain, where (2×1) domains with the surface atoms paired in the opposite way meet. Antiphase domains have also been observed in silicon epitaxy on Si(100)[37] at moderate temperatures. The (2×1) structure of Fig. 2 is presumably the so-called monohydride, with one hydrogen atom per surface carbon atom.[39,40]

A three-dimensional view of the surface topography of Sample IV is shown in Fig. 9. The (110)-oriented diamond film is very rough on the μm-mm scale, as observed by optical or electron microscopy.[9] A comparison of Figs. 9 and 3 shows that the morphology on the nm-μm scale is very different on the (110) and (100) films. The entire surface of the (110) film consists of hill-like features, ≈50-250 nm high and 100-800 nm wide, with no evidence of microfaceting. The total height variation in large-area scans was ≈500-1000 nm. The "hills" appear generally to be longer in one direction (near-vertical in Fig. 9) than in the orthogonal direction. The lateral dimensions of the

hills and their diverse detailed structures indicates that the structures are real and not simply images of the tip. The orientation of the images with respect to the underlying crystal lattice is unknown, but the existence of zig-zag chains of laterally-bonded surface carbon atoms in the $<1\bar{1}0>$ direction on ideal (110) surfaces suggests that this may be the "long" direction. Slopes as large as 46° were observed on the sides of the hills in the "narrow" direction, and slopes nearly as large are present in the "long" direction. The actual slopes may be somewhat larger due to the finite sharpness of the tip. The slopes are sufficiently large so that (100) and (111) planes are exposed locally on the surface: <100> lies 45° from <110> in the $<1\bar{1}0>$ direction and <111> lies 35.3° from <110> in the <001> direction. The absence of any observable faceting on the (110)-oriented film is therefore noteworthy, as polycrystalline films are almost always dominated by (111) and/or (100) facets. The local morphology of the "hilltops" is extremely smooth, as is evident in the 5×5 nm^2 scan shown in Fig. 10. However, although the peak-to-peak roughness is less than 2 Å, comparable to Sample III, no identifiable atomic features were observed.

Fig. 11 is a grey-scale AFM image of sample V showing the intersection of two cracks formed at different times during the growth of the film. Larger-area AFM images and optical micrographs of sample V showed cracks forming equilateral triangles and 60° parallelograms of various sizes. The six-fold symmetry of the cracks strongly suggests that the film is homoepitaxial, as spontaneous cleavage will occur on {111} planes, whose projections on the original (111) plane meet at 60° angles. Fracture took place after the film reached a critical thickness (≈ 3.5 μm)[9] and the sample was cooled and removed from the growth reactor for thickness measurements. An optical micrograph of a similarly-grown diamond (111) film has been reported previously.[9] Observation of interference fringes in optical micrographs with the sample lighted from below and occasional missing plates on the surface together indicate that fracture is accompanied by delamination of the film. Cleavage from the substrate does not occur at the original interface, as might be expected if nucleation was poor, as indicated by the roughness of surfaces exposed by the occasional loss of plates of the film. The near-horizontal crack in Fig. 11 formed at an early point in the growth of the film, with delamination and residual tensile stress causing the edges of the film to flex upwards. The sample was reinserted into the reactor and more diamond grown, resulting in "burial" of the crack and a more diffuse morphology. The sharpness of the second crack, running from the upper left to lower right, suggests that it formed immediately after the final film growth step. The portion of the film to the right of the second crack flexed upward more than the left-hand portion, resulting in the asymmetric appearance. Cross-sections of the steps near cracks indicated typical step heights of 20-200 nm.

The other noteworthy observation about the morphology of sample V is the degree of local roughness, both close to and far away from cracks. Smaller-area AFM scans taken near the centers

of the triangular plates (i.e., far from the cracks) show contiguous bumps with heights of 10-50 nm and widths of 30-100 nm. Cross-sectional measurements in regions far from any cracks revealed slopes as high as 39°; actual slopes may be somewhat larger due to convolution with the shape of the tip and the small lateral size of the features. However, no evidence of microfaceting was seen. We were unable to achieve a resolution higher than about 10 nm on this surface, perhaps due either to erosion of the tip or instabilities in the motion of the tip across the surface.

IV. DISCUSSION

A comparison of Figs. 2-7 demonstrates that growth conditions greatly affect the morphology of (100)-oriented diamond films on the nm-μm scale, just as they are responsible for well-documented variations in the micron-scale morphology of homoepitaxial diamond films[1-11] and diamond microcrystals and in the relative prevalence of (100) and (111) facets in polycrystalline films.[41-50] The variable morphology is consistent with the disparate results for (100)-oriented diamond growth reported by others, where (100) homoepitaxial films or (100) faces on microcrystals obtained under some conditions were smooth[2b,4,5,9,11,44,49,50] on the scale of the resolution of the instrument, whereas rough[1b,2b,3b,8,46,48] or even polycrystalline[1,3b] films were obtained under other conditions. While the present study demonstrates an effect of surface temperature and hydrocarbon mole fraction, further work will be necessary in order to precisely identify the aspects of the growth conditions responsible for specific features and the effects of the preexisting morphology and step density of the substrate and of the thickness of the film.

The morphological features of sample I are similar to features observed previously on CVD-grown diamond crystals or polycrystalline films on non-diamond substrates. Ledge formation during growth of (100) faces of individual diamond crystals has been seen by a number of groups by scanning electron microscopy (SEM),[44-47] and smooth-sided pyramids have also been observed.[46] Although the orientation of the pyramids on sample I with respect to the crystallographic orientation of the substrate was not determined, the pyramid bases probably lie parallel to $<01\bar{1}>$ or $<0\bar{1}1>$, since these are the most stable orientations of steps on Si(100),[35-37] and steps in the <010> orientation, for example, would be atomically rough and there would be no driving force to keep the step edge straight. Although Okada *et al.*[47] observed evidence of ledge growth due to a screw dislocation, spiral ledges are not evident in any of our AFM images and are absent in other reports of ledge growth of (100)-oriented diamond films,[44-46] and therefore screw dislocations seem unlikely to play any important role in determining the morphology seen on sample I. Pyramids with and without ledges have been observed immediately adjacent to one another, both on sample I and on diamond microcrystals,[46] implying that growth can proceed along <100> or be

tilted off-<100> by a few degrees by subtle differences in substrate and/or gas-phase conditions To our awareness, penetration twins on (100) diamond films have been reported to date only by Clausing *et al.*[34] Further work, both experimental and theoretical, will be necessary in order to understand the precise factors responsible for the generation of pyramids and penetration twins.

The observation of essentially flat (100) surfaces following growth at higher substrate temperatures (Figs. 5-7), particularly at higher hydrocarbon flow rates, implies that growth occurs predominantly at steps, ledges, or kinks, or at least that extension of lattice planes occurs much faster than nucleation of a new layer. If this were not true, the surfaces would be much rougher on the nm scale due to nucleation and growth of new layers randomly across the surface. The fact that sample III is much flatter than sample II (terrace widths of ≈ 20 and ≈ 0.7 nm, respectively) implies that the ratio of the rate of step extension to that of nucleation of a new layer increases considerably as the hydrocarbon mole fraction and substrate temperature are increased.

Although the evidence for (2×1) dimer rows in Fig. 7 is admittedly less than compelling, we believe the features to be real, and similar observations of a (2×1) reconstruction on as-grown diamond (100) films by a number of other laboratories lead us to propose that in fact diamond (100) faces are predominantly covered by (2×1) dimer rows under CVD growth conditions. The structural model in Fig. 8 for the dimer rows in Fig. 7 is completely consistent with the AFM image: the spacing between the rows is correct, the cubic crystalline symmetry is correct, and the dimer rows on the terrace one atomic spacing higher are rotated by 90° as they should be. Generation of a spurious image by tip effects seems unlikely, as Si_3N_4 is not a cubic material and does not have structural features separated by 5 Å. The STM images of CVD-grown diamond (100) by Tsuno *et al.*[26] are significantly clearer than Fig. 7, and their observations of dimer rows, type A and B single steps and type A double steps[35] seem beyond dispute. Tsuno *et al.*[26] did not report an antiphase domain of the type shown in Fig. 7, but such a structural feature is likely to be growth-condition-dependent. Tsuno *et al.*[26] obtained further evidence of the (2×1) reconstruction by reflection high energy electron diffraction (RHEED) following growth and transfer of the sample in air, and a similar observation was made by Thomas *et al.*[51] by low energy electron diffraction (LEED), again following an air transfer. Finally, Sprang *et al.*[52] have also very recently reported observation of (2×1) dimer rows on a strongly-(100)-textured polycrystalline diamond film by STM. The dimerized surface carbon atoms most likely exist in the monohydride configuration, with one hydrogen atom bonded to each atom in the dimer, since the structure is air-stable and samples are likely to be exposed to atomic hydrogen during the shutdown of the growth reactor.

The observation of (2×1)-reconstructed diamond (100) surfaces by a number of workers, whose growth conditions presumably varied considerably, suggests that a dimerized surface structure dominates under CVD growth conditions rather than the more widely discussed (1×1):2H

dihydride.[17a,39] Theoretical support for this conclusion comes from the molecular mechanics calculations of Yang and D'Evelyn,[40,53] who found that the monohydride is the most stable high-symmetry phase over the temperature range of 298-1500 K, followed in stability by the clean surface, which also consists of (2×1)-reconstructed dimers. The (1×1):2H dihydride was found to be thermodynamically unstable with respect to dehydrogenation due to extreme steric repulsion between nonbonded surface hydrogen atoms.[40,53] While observation of a surface structure after growth and air exposure does not prove that the structure was present under growth conditions, it is strongly suggestive, particularly when that structure is a stable one and its appearance is insensitive to the details of growth and reactor shutdown conditions, as evidenced by its observation in different laboratories. Since less-stable structures like the (1×1):2H full dihydride and the (3×1):1.33H partial dihydride[40,53] are favored at lower temperatures, if they did exist under growth conditions they would likely be stable as growth was quenched and the substrate was cooled. The fact that they have not been observed provides indirect evidence that they also do not exist in large concentrations under growth conditions and that the (2×1):H monohydride predominates, with clean (2×1) dimers perhaps also being important.

An additional argument for the existence of a (2×1) reconstruction on diamond (100) under growth conditions follows from the observed smoothness of the film surfaces. The periodic bond chain (PBC) theory of Hartman[54] relates the predicted smoothness and growth rates of particular crystal faces to the number of bonds each surface unit (atom) has with neighboring surface units, and successfully accounts for observed morphologies of many types of crystals grown by a wide variety of methods. However, application of the Hartman theory to the unreconstructed (100) surface of the diamond-structure lattice leads to the prediction of rough surfaces,[54] which is contradicted by the smoothness of (100)-oriented films not only of diamond but also of silicon, germanium, and gallium arsenide grown under wide-ranging conditions.[55] Giling and van Enckevort[55] showed that the contradiction could be resolved by assuming that (2×1) reconstructions are present during growth, with the dimer bonds supplying the missing surface bonds required by the PBC theory for smoothness. Their analysis assumes that the other unsatisfied valence on each (100) surface atom remains a dangling bond, whereas under diamond CVD conditions most dangling bonds are probably capped by chemisorbed hydrogen, forming the monohydride. However, the same argument applies as long as the step energy is positive, that is, formation of atomic steps costs energy, and therefore should be applicable to (100)-oriented diamond growth. On the other hand, the extreme steric hindrance in the (1×1):2H dihydride[40] is greatly reduced when dihydride units are not adjacent to one another,[40,53] suggesting that step formation on a dihydride-terminated surface would instead *lower* the surface energy. The negative step energy associated with the dihydride surface would predict extremely rough surfaces by the inverse of the argument of Giling and van Enckevort,[55] which is contradicted by the observed

smoothness of the surfaces.

All CVD-grown, (110)-oriented homoepitaxial diamond film surfaces that have been characterized and reported to date have been rough on the μm scale.[2b,3b,4-10] (110) facets have only rarely been observed on CVD-grown diamond crystals.[49,50] However, the present results are the first to show their morphology on the nm scale. The observation of a high degree of corrugation, with local slopes as high as 45° yet no microfaceting, is striking. The lack of faceting indicates that (110)-oriented growth is stable, in a sense, since the [100] and [111] orientations were exposed without becoming dominant. Only a distinct minority of the surface, however, has an orientation vicinal to <110>. Fig. 10 demonstrates that the film is extremely smooth on the nm scale, at least on top of the "hills," suggesting that the gross morphology is built up from one- or few-atom-high steps and kinks and that growth occurs preferentially at these low-coordination sites. The relatively random direction of the slopes provides fairly strong evidence for steps of widely varying orientation, even though they were not observed directly, which in turn implies that growth occurs at sites of varying local structure, not just at a single type of site.

Spontaneous fracture of (111)-oriented diamond films has been described by at least one other set of authors.[3] We have shown previously[9] that the cracking of is a consequence of tensile stress, evidenced by a stress-shifted Raman peak in thin, (111)-oriented ^{13}C diamond films which relaxed to the unstressed value as the film thickness was increased sufficiently (to ≈ 3.5 μm) to induce spontaneous fracture. As noted above, fracture occurred after cooling and removal of the sample from the reactor. This suggests that the stress may actually be *thermal*, arising from unequal thermal expansion coefficients of substrate and film, with the film having the larger value so that tensile stress arises upon cooling from the growth temperature. It is not clear whether the stress is isotropic across the film, but no evidence was seen for splitting of the normally triply-degenerate Raman peak and only a minor decrease in linewidth occurred upon fracture.[9] The shift of the Raman peak frequency can therefore be used to estimate the stress in films prior to cracking. Using the reported pressure coefficient of the Raman frequency, 2.75 cm^{-1} GPa^{-1},[56] the observed shift of -5.1 cm^{-1} [9] corresponds to a stress of about 1.9 GPa. The film contracts by roughly 0.18% relative to the substrate upon fracture, using the biaxial Young's modulus of diamond of 1050 GPa,[57] which corresponds to a mean difference in thermal expansion coefficients between film and substrate of $\approx 1.9 \times 10^{-6}$ K^{-1}. This value is a sizable fraction of the mean value of the thermal expansion coefficient of diamond over the range of 25–966 °C, $\approx 3 \times 10^{-6}$ K^{-1}, [58] indicating that the mechanical properties of the film are strongly perturbed. The difference also suggests that the modulus of the film is also significantly different from bulk diamond, implying that the calculations just given should be regarded as rough estimates only. The cause of the increased thermal expansion coefficient in the (111) film is not clear, but Raman spectra indicate some incorporation

of graphitic carbon into the film, and several authors have shown that stacking-fault formation and twinning are ubiquitous in (111)-oriented growth,[34,43b,59-61] and either of these factors may be responsible.

Rough local morphologies have been reported on virtually all the (111) diamond epilayers that have been grown[1c,3b,4,8] and are also typically observed on (111) facets of polycrystalline films and individual crystals.[42,49,50] The detailed local structure is of obvious relevance to the growth mechanism. The range of observed slopes on the surface of sample V suggests that growth occurred at sites of varying structure, most likely steps. The short lateral range of the roughness (≈ 30-100 nm) provides indirect support for proposals of propagation of defect structures in [111] growth,[27,34,62] and the implication of growth predominantly at non-(111)-like sites agrees with the calculations of Harris *et al.*,[63] who concluded that simple hydrocarbon addition reactions to a flat (111) surface could not account for observed growth rates. However, the fairly amorphous "bump" structure observed in this study is rather different than the triangular tiles and pits ≈ 15-40 nm in size observed recently on (111) facets of CVD-grown diamond microcrystals by Hirabayashi and Kurihara[50] using high-resolution SEM. The difference may be due to some incorporation of graphitic carbon in our films or, alternatively, to a sensitivity of the nanometer-scale morphology in (111)-oriented growth to differences in the growth conditions, as we have shown occurs for (100)-oriented growth.

It seems appropriate to punctuate the above comments on morphological similarities between homoepitaxial diamond films and facets of diamond crystals with a *caveat.* Existing evidence suggests that the sub-micron morphology of individual crystal faces on CVD-grown diamond microcrystals or polycrystalline films will normally *not* be directly analogous to the local structure of a homoepitaxial film of the same orientation. Several authors have reported differences in the local morphologies of the centers and edges of facets on CVD-grown diamond microcrystals.[49,50] In addition, the local morphology of diamond microcrystals has also been shown to depend on the substrate,[64,65] e.g., mechanically-polished Mo, MoC, and diamond-like carbon.[65] These differences may result from perturbation of the gas-phase chemistry by the substrate, changing the local concentrations of the reactants. Such a perturbative effect has recently been demonstrated by Hsu,[12g] who showed that surface recombination of atomic hydrogen at the diamond surface strongly affects the gas-phase H concentration near the substrate, in agreement with the predictions of Goodwin and Gavillet.[66] The surface recombination rate of hydrogen, which is due to abstraction of surface hydrogen by incident atomic hydrogen, is almost certainly different on different substrates and may show significant differences on the different crystal faces of diamond. Given the importance of atomic hydrogen in determining the local concentration of CH_3,[12] the demonstrated importance of CH_3 in diamond CVD,[13,14] and the probable role of atomic hydrogen

in driving surface reactions,[15-20] the effect just cited could well explain the observed differences in local morphology. Another possible cause or contributing factor may be local stress effects. Since (111)-oriented growth is accompanied by copious stacking-faults and twins[4,34,43b,59-61] whereas (100)-oriented growth is comparatively defect-free,[4,61] the edge regions of facets are likely to possess strain fields which are absent in the centers and affect the local surface morphology. Study of surface morphology on the nanometer-to-micron scale is therefore best done with *homoepitaxial* diamond films, where complications in the gas-phase chemistry and substrate properties are kept to a minimum.

Our results have implications for detailed diamond CVD growth models. As disparate growth models predict growth rates in reasonable agreement with experiment, it is clear that much more experimental input is necessary in order to discriminate between them and to establish the key steps in growth. We have demonstrated that growth conditions exert a significant effect on the nm-scale morphology, which is much more amenable to theoretical simulation than larger-scale structures. Growth models proposed to date focus on different crystal faces, including (100)-(1×1),[16e,17a] (100)-(2×1),[16e,20] (110),[17c,18] flat (111),[15,17b,19] and (111) with (100)-like[17d] or (110)-like[16] steps. We have argued above that a (2×1) reconstruction predominates on (100) surfaces under typical hot-filament CVD conditions and that growth occurs predominantly at sites of reduced coordination number, such as steps. Several authors have proposed microstructural effects associated with growth on diamond (110), including suggestions that (110) microfacets exist on faces of nominal (111)[49] or (100) orientation,[18] or that (110)-oriented growth is accompanied by (111)-microtwinning.[8] The present results do not support these suggestions, as no evidence for micro- or nano-faceting was seen on (100), (110), or (111) epilayers, and the local orientation of a (110) epitaxial film was seen to vary smoothly from <110> to <100> and <111> and beyond. The development of <110> textures in polycrystalline diamond films appears to be a simple consequence of growth rates in different crystallographic directions,[34,61,67,68] requiring no special role for the (110) face. Although detailed growth models have not yet been applied to long-term simulation of atomic-scale morphologies, it seems likely that the predictions of different models will differ qualitatively, offering an improved basis for discriminating between them. Therefore it seems reasonable to ask detailed growth models to move beyond description of the initial stages of addition to the diamond lattice and estimation of growth rates to prediction of local surface morphologies of many-monolayer-thick films for comparison with experiment.

CONCLUSIONS AND SUMMARY

We have studied the surface topography on the nanometer-to-micron scale of homoepitaxial diamond films grown by hot filament CVD conditions using atomic force microscopy. It is evident from the results that AFM can provide a wealth of information on the CVD growth of diamond films. Our principal observations may be summarized as follows:

(i) (100) epitaxial films displayed a growth-condition-dependent morphology: rough on the μm scale with pyramidal features and penetration twins at a substrate temperature of 810 °C and low CH_4 flow rate; nearly atomically smooth at 1000 °C and higher hydrocarbon flow rate.

(ii) Evidence for a dimer-type (2×1) reconstruction on a smooth (100) surface was found.

(iii) A (110) epitaxial film was very rough (> 100 nm) on the >100 nm scale but nearly atomically smooth on the 0.5-5 nm scale and exhibited local slopes higher than 40° with no evidence of microfaceting.

(iv) A (111) epitaxial film with some graphitic content fractured due to tensile stress and displayed ≈10-50 nm roughness on the 10-500 nm scale.

(v) The observed smoothness of the films on the nanometer scale indicates that diamond growth is fastest at low-coordination-number sites.

ACKNOWLEDGMENTS

The authors acknowledge the National Science Foundation for support of this work by Grant CHE-8807546 and the Office of Naval Research and Shell Development Co. for additional support. The authors thank Dr. David Denley for use of his Nanoscope II computer and for helpful comments, and Dr. Steve Harris, Dr. Michael Frenklach, and Dr. Barbara Garrison for providing us with manuscripts prior to publication.

REFERENCES

1. (a) B. V. Derjaguin, B. V. Spitsyn, A. E. Aleksenko, A. E. Gorodetsky, A. P. Zakharov, and R. I. Nazarova, Dokl. Akad. Nauk SSSR **213**, 1059 (1973) [Sov. Phys. Dokl. **18**, 822 (1974)]; (b) B. V. Derjaguin, B. V. Spitsyn, A. E. Gorodetsky, A. P. Zakharov, L. L Bouilov, and A. E. Aleksenko, J. Cryst. Growth **31**, 44 (1975); (c) B. V. Spitsyn, L. L. Bouilov, and B. V. Derjaguin, J. Cryst. Growth **52**, 219 (1981).
2. (a) N. Fujimori, T. Imai, and A. Doi, Vacuum **36**, 99 (1986); (b) H. Shiomi, K. Tanabe, Y. Nishibayashi, and N. Fujimori, Jpn. J. Appl. Phys. **29**, 34 (1990); (c) N. Fujimori, H. Nakahata, and T. Imai, Jpn. J. Appl. Phys. **29**, 824 (1990).
3. (a) H. Nakazawa, Y. Kanazawa, M. Kamo, and K. Osumi, Thin Solid Films **151**, 199 (1987); (b) M. Kamo, H. Yurimoto, and Y. Sato, Appl. Surf. Sci. **33/34**, 553 (1988).
4. M. Geis, Mater. Res. Soc. Symp. Proc. **162**, 15 (1990).
5. A. R. Badzian, T. Badzian, X. H. Wang, and T. M. Hartnett, in *New Diamond Science and Technology*, edited by R. Messier, J. T. Glass, J. E. Butler, and R. Roy (Materials Research Society, Pittsburgh, PA, 1991), p. 549.
6. K. Okano, Y, Akiba, T. Kurosu, M. Iida, and T. Nakamura, J. Cryst. Growth **99**, 1192 (1990).
7. G. Janssen, W. J. P. van Enckevort, J. J. D. Schaminée, W. Vollenberg, L. J. Giling, and M. Seal, J. Cryst. Growth **104**, 752 (1990).
8. J. F. DeNatale, A. B. Harker, and J. F. Flintoff, J. Appl. Phys. **69**, 6456 (1991).
9. C. J. Chu, M. P. D'Evelyn, R. H. Hauge, and J. L. Margrave, J. Appl. Phys. **70**, 1695 (1991).
10. K. A. Snail and L. M. Hanssen, J. Cryst. Growth **112**, 651 (1991).
11. J. B. Posthill, R. A. Rudder, G. C. Hudson, D. P. Malta, G. G. Fountain, R. E. Thomas, R. J. Markunas, T. P. Humphreys, R. J. Nemanich, and D. R. Black, in *Diamond Materials*, edited by A. J. Purdes, J. C. Angus, R. F. Davis, B. M. Meyerson, K. E. Spear, and M. Yoder (The Electrochemical Society, Pennington, New Jersey, 1991), p. 274.
12. (a) F. G. Celii and J. E. Butler, Annu. Rev. Phys. Chem. **42**, 643 (1991) and references therein; (b) S. J. Harris, A. M. Weiner, and T. A. Perry, Appl. Phys. Lett. **53**, 1605 (1988); (c) M. Frenklach, J. Appl. Phys. **65**, 5142 (1989); (d) S. J. Harris and A. M. Weiner, J. Appl. Phys. **67**, 6520 (1990); (e) C.-H. Wu, M. A. Tamor, T. J. Potter, and E. W. Kaiser, J. Appl. Phys. **68**, 4825 (1990); (f) D. G. Goodwin and G. G. Gavillet, J. Appl. Phys. **68**, 6393 (1990); (g) W. L. Hsu, Appl. Phys. Lett. **59**, 1427 (1991).

13. (a) C. J. Chu, M. P. D'Evelyn, R. H. Hauge, and J. L. Margrave, J. Mater. Res. **5**, 2405 (1990); (b) M. P. D'Evelyn, C. J. Chu, R. H. Hauge, and J. L. Margrave, "Mechanism of diamond growth by hot-filament chemical vapor deposition: Carbon-13 studies," J. Appl. Phys. (in press).

14. (a) L. R. Martin and M. W. Hill, J. Mater. Sci. Lett. **9**, 621 (1990); (b) S. J. Harris and L. R. Martin, J. Mater. Res. **5**, 2313 (1990).

15. (a) M. Tsuda, M. Nakajima, and S. Oikawa, J. Am. Chem. Soc. **108**, 5780 (1986); (b) M. Tsuda, M. Nakajima, and S. Oikawa, Jpn. J. Appl. Phys. **26**, L527 (1987).

16. (a) M. Frenklach and K. E. Spear, J. Mater. Res. **3**, 133 (1988); (b) D. Huang, M. Frenklach, and M. Maroncelli, J. Phys. Chem. **92**, 6379 (1988); (c) M. Frenklach and H. Wang, Phys. Rev. B **43**, 1520 (1991); (d) D. Huang and M. Frenklach, J. Phys. Chem. **95**, 3692 (1991); (e) D. Huang and M. Frenklach, "Energetics of surface reactions on (100) diamond plane," J. Phys. Chem. (in press).

17. (a) S. J. Harris, Appl. Phys. Lett. **56**, 2298 (1990); (b) S. J. Harris, D. N. Belton, and R. J. Blint, J. Appl. Phys. **70**, 2654 (1991); (c) D. N. Belton and S. J. Harris, "Growth from acetylene on the diamond (110) surface," J. Chem. Phys. (in press); (d) S. J. Harris and D. N. Belton, "Diamond growth on a (100)-type step," submitted to Thin Solid Films..

18. W. A. Yarbrough, in *Diamond Optics IV*, edited by S. Holly and A. Feldman (SPIE Proc. 1534, Bellingham, WA) (in press).

19. P. Deák, J. Giber, and H. Oechsner, Surf. Sci. **250**, 287 (1991).

20. B. J. Garrison and D. W. Brenner, "Molecular-dynamics simulations of hydrocarbon reactions: Suggested mechanism for initial stages of diamond film formation on a reconstructed (100) surface," Science (in press).

21. K. F. Turner, B. R. Stoner, L. Bergman, J. T. Glass, and R. J. Nemanich, J. Appl. Phys. **69**, 6400 (1991).

22. H.-G. Busmann, H. Sprang, I. V. Hertel, W. Zimmermann-Edling, and H.-J. Güntherodt, Appl. Phys. Lett. **59**, 295 (1991).

23. L. H. Robins, E. P. Whitenton, E. N. Farabaugh, and A. Feldman, in *New Diamond Science and Technology*, edited by R. Messier, J. T. Glass, J. E. Butler, and R. Roy (Materials Research Society, Pittsburgh, PA, 1991), p. 619.

24. M. P. Everson, M. A. Tamor, and C. H. Wu, in *New Diamond Science and Technology*, edited by R. Messier, J. T. Glass, J. E. Butler, and R. Roy (Materials Research Society, Pittsburgh, PA, 1991), p. 613.

25. A. W. Phelps and T. W. Owens, in *Diamond Materials*, edited by A. J. Purdes, J. C. Angus, R. F. Davis, B. M. Meyerson, K. E. Spear, and M. Yoder (The Electrochemical Society, Pennington, New Jersey, 1991), p. 502.

26. T. Tsuno, T. Imai, Y. Nishibayashi, K. Hamada, and N. Fujimori, Jpn. J. Appl. Phys. **30**, 1063 (1991).

27. J. C. Angus, Z. Li, M. Sunkara, R. Gat, A. B. Anderson, S. P. Mehandru, and M. W. Geis, in *Diamond Materials*, edited by A. J. Purdes, J. C. Angus, R. F. Davis, B. M. Meyerson, K. E. Spear, and M. Yoder (The Electrochemical Society, Pennington, New Jersey, 1991), p. 125.

28. L. F. Sutcu, M. S. Thompson, C. J. Chu, R. H. Hauge, J. L. Margrave, and M. P. D'Evelyn, "Nanometer-scale morphology of homoepitaxial diamond films by atomic force microscopy," submitted to Appl. Phys. Lett.

29. C. J. Chu, R. H. Hauge, J. L. Margrave, and M. P. D'Evelyn, to be published.

30. R. J. Nemanich, J. T. Glass, G. Lucovsky, and R. E. Shroder, J. Vac. Sci. Technol. A **6**, 1783 (1988)

31. D. S. Knight and W. B. White, J. Mater. Res. **4**, 385 (1989).

32. J. Wagner, M. Ramsteiner, Ch. Wild, and P. Koidl, Phys. Rev. B **40**, 1817 (1989).

33. For example, A. M. Cody and R. D. Cody, J. Cryst. Growth **83**, 485 (1987), and references therein.

34. R. E. Clausing, L. Heatherly, E. D. Specht, and K. L. More, in *New Diamond Science and Technology*, edited by R. Messier, J. T. Glass, J. E. Butler, and R. Roy (Materials Research Society, Pittsburgh, PA, 1991), p. 575.

35. D. J. Chadi, Phys. Rev. Lett. **59**, 1691 (1987).

36. R. J. Hamers, R. M. Tromp, and J. E. Demuth, Phys. Rev. B **34**, 5343 (1986).

37. R. J. Hamers, U. K. Kohler, and J. E. Demuth, J. Vac. Sci. Technol. A **8**, 195 (1990).

38. J. A. Kubby, J. E. Griffith, R. S. Becker, and J. S. Vickers, Phys. Rev. B **36**, 6079 (1987).

39. A. V. Hamza, G. D. Kubiak, and R. H. Stulen, Surf. Sci. **237**, 35 (1990).

40. Y. L. Yang and M. P. D'Evelyn, "Structure and energetics of clean and hydrogenated diamond (100) surfaces by molecular mechanics," J. Am. Chem. Soc. (in press).

41. J. C. Angus and C. C. Hayman, Science **241**, 913 (1988).

42. W. A. Yarbrough and R. Messier, Science **247**, 688 (1990).

43. (a) S. Matsumoto, Y. Sato, M. Tsutsumi, and N. Setaka, J. Mater. Sci. **17**, 3106 (1982); (b)

S. Matsumoto and Y. Matsui, J. Mater. Sci. **18**, 1785 (1983).

44. K. Kobashi, K. Nishimura, Y. Kawate, and T. Horiuchi, Phys. Rev. B **38**, 4067 (1988).
45. K. V. Ravi and A. Joshi, Appl. Phys. Lett. **58**, 246 (1991).
46. H. Itoh, T. Nakamura, H. Iwahara, and H. Sakamoto, in *New Diamond Science and Technology*, edited by R. Messier, J. T. Glass, J. E. Butler, and R. Roy (Materials Research Society, Pittsburgh, PA, 1991), p. 479, and J. Cryst. Growth **108**, 647 (1991). (they also see trigon, pits on 111)
47. K. Okada, S. Komatsu, S. Matsumoto, and Y. Moriyoshi, J. Cryst. Growth **108**, 416 (1991).
48. S. J. Harris, A. M. Weiner, and T. A. Perry, J. Appl. Phys. **70**, 1385 (1991).
49. J. S. Kim, M. H. Kim, S. S. Park, and J. Y. Lee, J. Appl. Phys. **67**, 3354 (1990).
50. K. Hirabayashi and N. I. Kurihara, Jpn. J. Appl. Phys. **29**, L1862 (1990) and **29**, L1901 (1990).
51. R. E. Thomas, R. A. Rudder, and R. J. Markunas, in *Diamond Materials*, ed. A. J. Purdes, J. C. Angus, R. F. Davis, B. M. Meyerson, K. E. Spear, and M. Yoder (The Electrochemical Society, Pennington, New Jersey, 1991), p.186.
52. H. Sprang, H.-G. Busmann, I. V. Hertel, W. Zimmermann-Edling, and H.-J. Güntherodt, presentation at the Second European Conference on Diamond, Diamond-like and Related Coatings (Nice, France, September 1991).
53. Y. L. Yang and M. P. D'Evelyn, "Theoretical studies of clean and hydrogenated diamond (100) by molecular mechanics," J. Vac. Sci. Technol. A (in press).
54. P. Hartman and W. G. Perdok, Acta Cryst. **8**, 49, 521 (1955); P. Hartman, in *Crystal Growth: An Introduction*, edited by P. Hartman (North-Holland, Amsterdam, 1973), p. 367.
55. L. J. Giling and W. J. P. van Enckevort, Surf. Sci. **161**, 567 (1985).
56. Mean of values reported by: (a) E. Whalley, A. Lavergne, and P. T. T. Wong, Rev. Sci. Instrum. **47**, 845 (1976); (b) S. L. Sharma, H. K. Mao, P. M. Bell, and J. A. Xu, J. Raman Spectrosc. **16**, 350 (1985); (c) M. Hanfland, K. Syassen, S. Fahy, S. G. Louie, and M. L. Cohen, Phys. Rev. B **31**, 6896 (1985); (d) H. Boppart, J. Van Straaten, and I. F. Silvera, Phys. Rev. B **32**, 1423 (1985); (e) A. Tardieu, F. Cansell, and J. P. Petitet, J. Appl. Phys. **68**, 3243 (1990).
57. (a) H. J. McSkimin and P. Andreatch, J. Appl. Phys. **43**, 985, 2944 (1972); (b) M. H. Grimsditch and A. K. Ramdas, Phys. Rev. B **11**, 3139 (1975).

58. G. A. Slack and S. F. Bartram, J. Appl. Phys. **46**, 89 (1975).

59. B. E. Williams, J. T. Glass, R. F. Davis, and K. Kobashi, J. Cryst. Growth **99**, 1168 (1990).

60. J. Narayan, J. Mater. Res. **5**, 2414 (1990).

61. Z. L. Wang, J. Bentley, R. E. Clausing, L. Heatherly, and L. L. Horton, in *Applications of Diamond Films and Related Materials*, edited by Y. Tzeng, M. Yoshikawa, M. Murakawa, and A. Feldman (Elsevier, Amsterdam, 1991), p. 489.

62. (a) J. C. Angus, R. W. Hoffman, and P. H. Schmidt, in *Proc. First Intl. Conf. New Diamond Science and Technology* (KTK Scientific Publishing, Tokyo, 1991); (b) J. C. Angus, F. A. Buck, M. Sunkara, T. F. Groth, C. C. Hayman, and R. Gat, MRS Bulletin, 38 (October 1989); (c) M. Sunkara, J. C. Angus, C. C. Hayman, and F. A. Buck, Carbon **28**, 745 (1990).

63. S. J. Harris, D. N. Belton, and R. J. Blint, J. Appl. Phys. **70**, 2654 (1991).

64. K. Kobashi, K. Nishimura, K. Miyata, K. Kumagai, and A. Makaue, J. Mater. Res. **5**, 2469 (1990).

65. K. V. Ravi, C. A. Koch, H. S. Hu, and A. Joshi, J. Mater. Res. **5**, 2356 (1990).

66. D. G. Goodwin and G. G. Gavillet, in *New Diamond Science and Technology*, edited by R. Messier, J. T. Glass, J. E. Butler, and R. Roy (Materials Research Society, Pittsburgh, PA, 1991), p. 335.

67. (a) Ch. Wild, N. Herres, and P. Koidl, J. Appl. Phys. **68**, 973 (1990); (b) C. Wild, P. Koidl, N. Herres, W. Müller-Sebert, and T. Eckerman, in *Diamond Materials*, edited by A. J. Purdes, J. C. Angus, R. F. Davis, B. M. Meyerson, K. E. Spear, and M. Yoder (The Electrochemical Society, Pennington, New Jersey, 1991), p. 224.

68. E. D. Specht, R. E. Clausing, and L. Heatherly, J. Mater. Res. **5**, 2351 (1990).

Tables

Table I. Experimental conditions for growth of homoepitaxial diamond films characterized by atomic force microscopy.

	Diamond samples (type 2A substrates)				
	I	II	III	IV	V
Substrate orientation	(100)	(100)	(100)	(110)	(111)
Substrate growth temperature (°C)	810	850	1000	850	966
Film thickness (mm)	2.9	2	12	5.1	9.2
Substrate heater (0.06 mm thick foil)	Mo	Pt	Pt	Pt	Pt
H_2 flow (sccm, over filaments)	168	179	176	179	152
H_2 flow (sccm, with hydrocarbons)*	10	11	10	11	-
CH_4 flow (sccm)*	0.5	0.3	3	0.3	0.3 -1.3
C_2H_2 flow (sccm)*	0.00	0.15	0.00	0.15	0.00
Filament temperature (°C)	2010	2000	2125	2000	2160

* Introduced below the tungsten filaments[13a] except in the case of Sample V, which was introduced over the filaments.

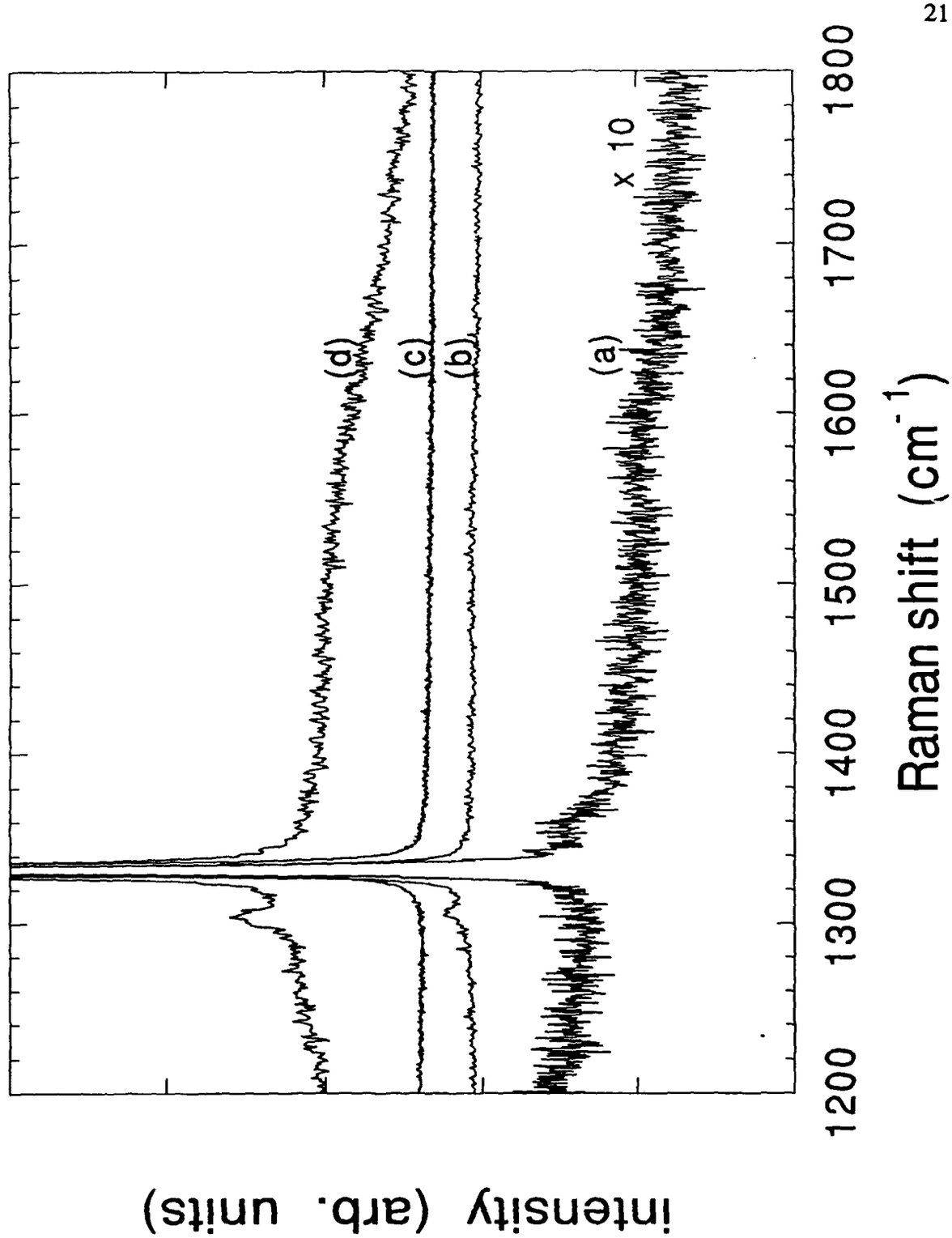

Fig. 1. Representative Raman spectra of (a) sample I, (b) sample II, (c) sample III, and (d) sample IV.

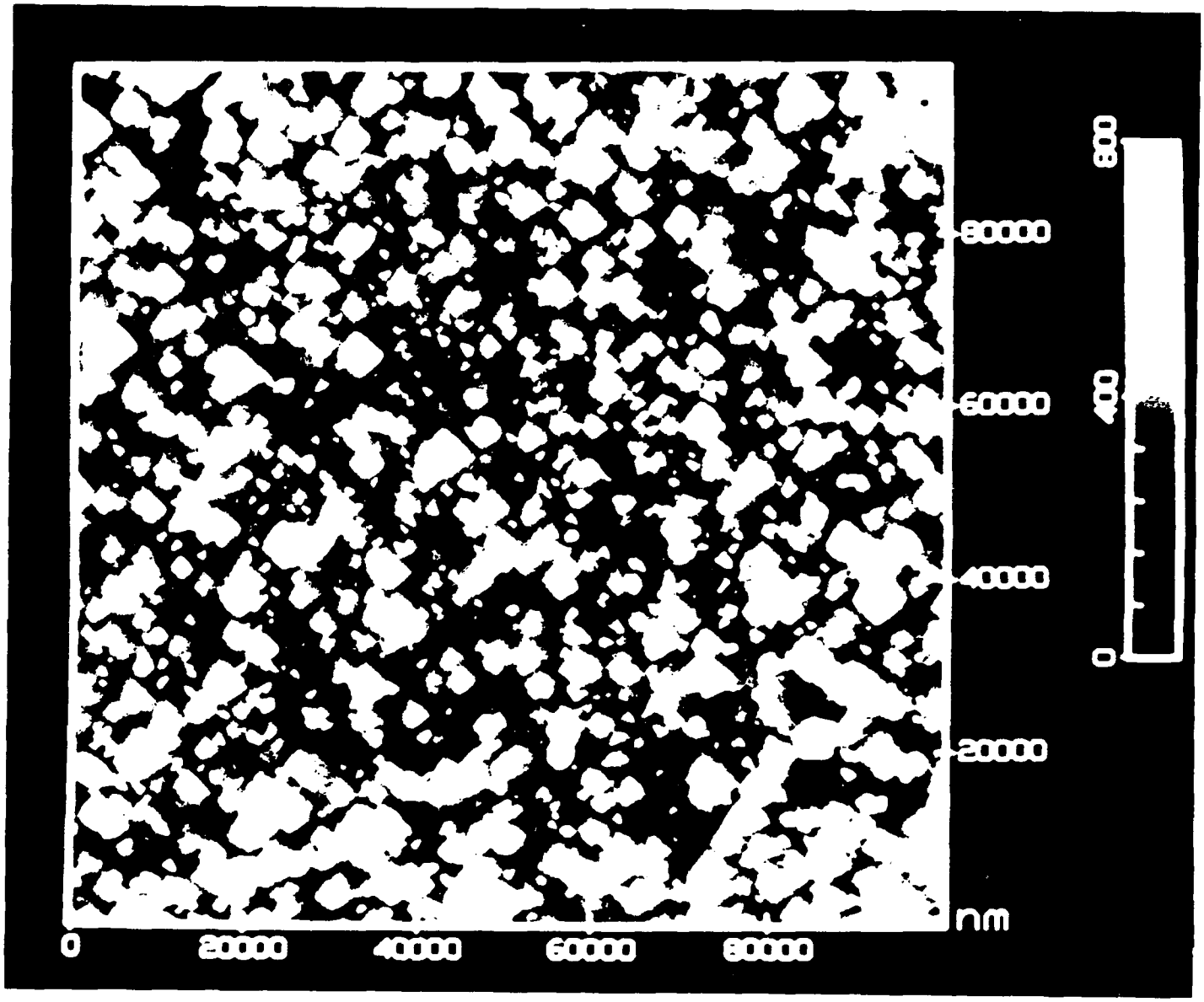

Fig. 2. $100 \times 100\ \mu m^2$ AFM scan of epitaxial diamond (100) film (sample I).

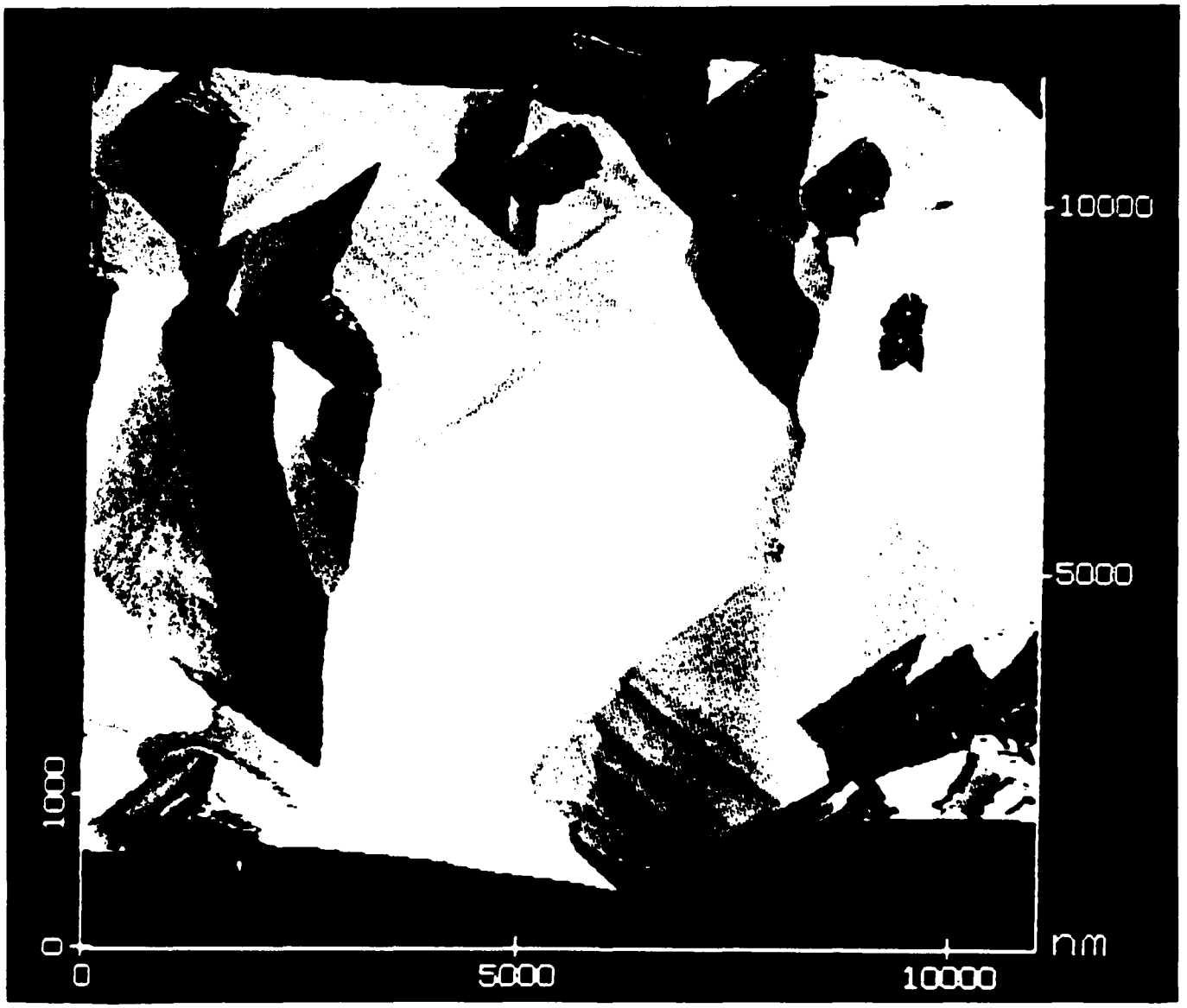

Fig. 3. Three-dimensional view of pyramids and penetration twins on the faceted (100) surface (sample I).

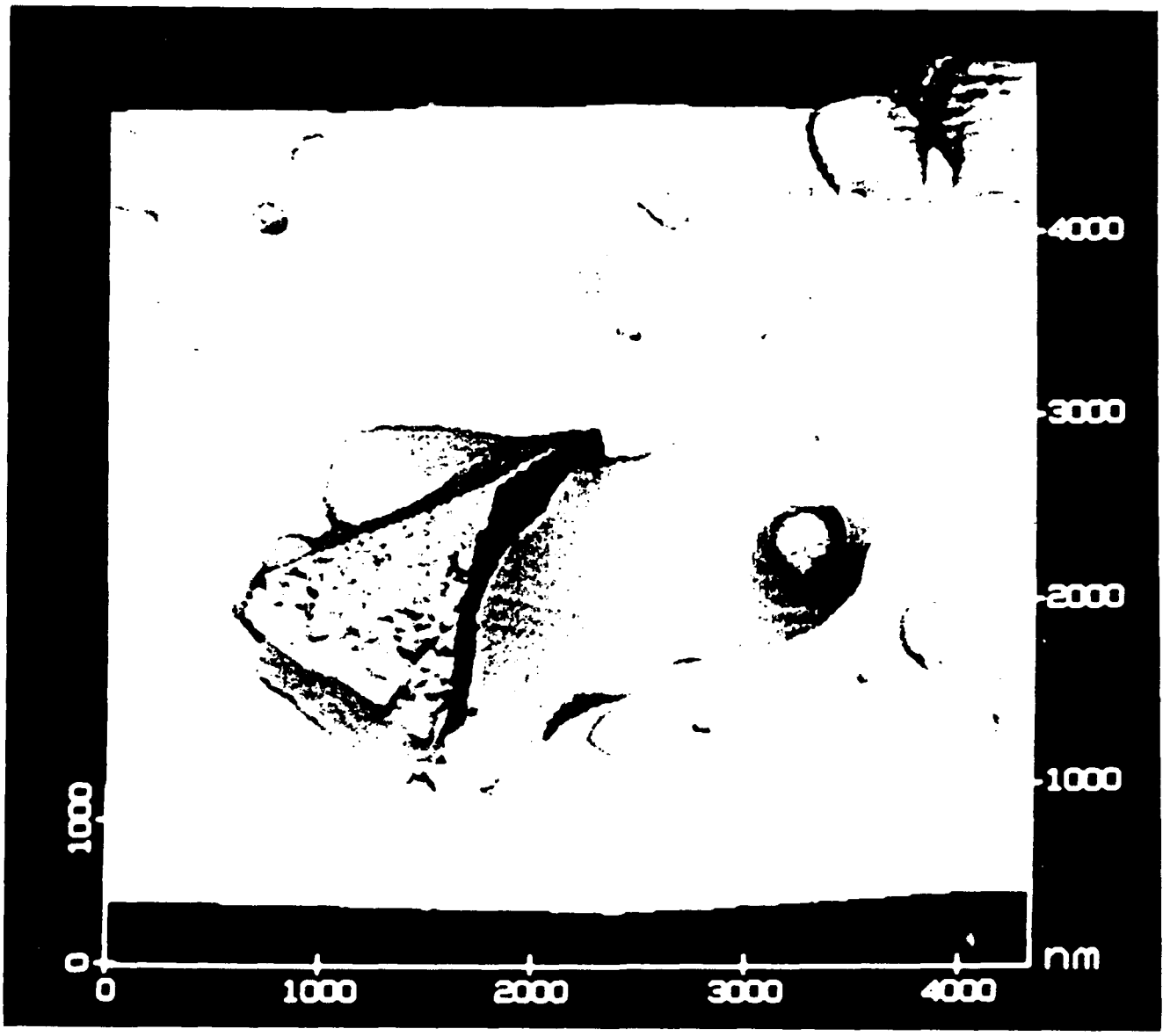

Fig. 4. Three-dimensional view of an isolated penetration twin on the faceted (100) surface (sample I).

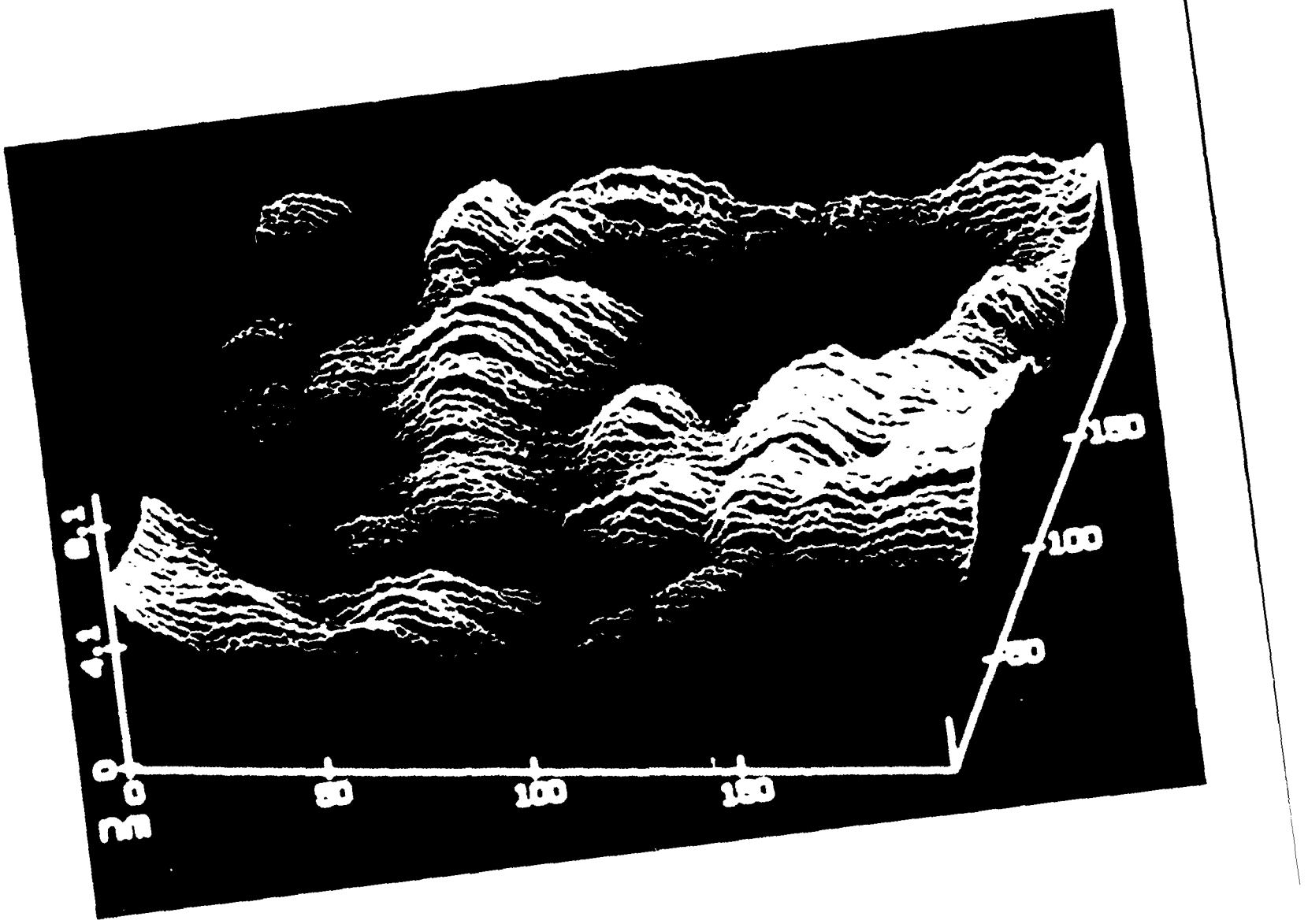

Fig. 5. AFM image of epitaxial (100) diamond film (sample II).

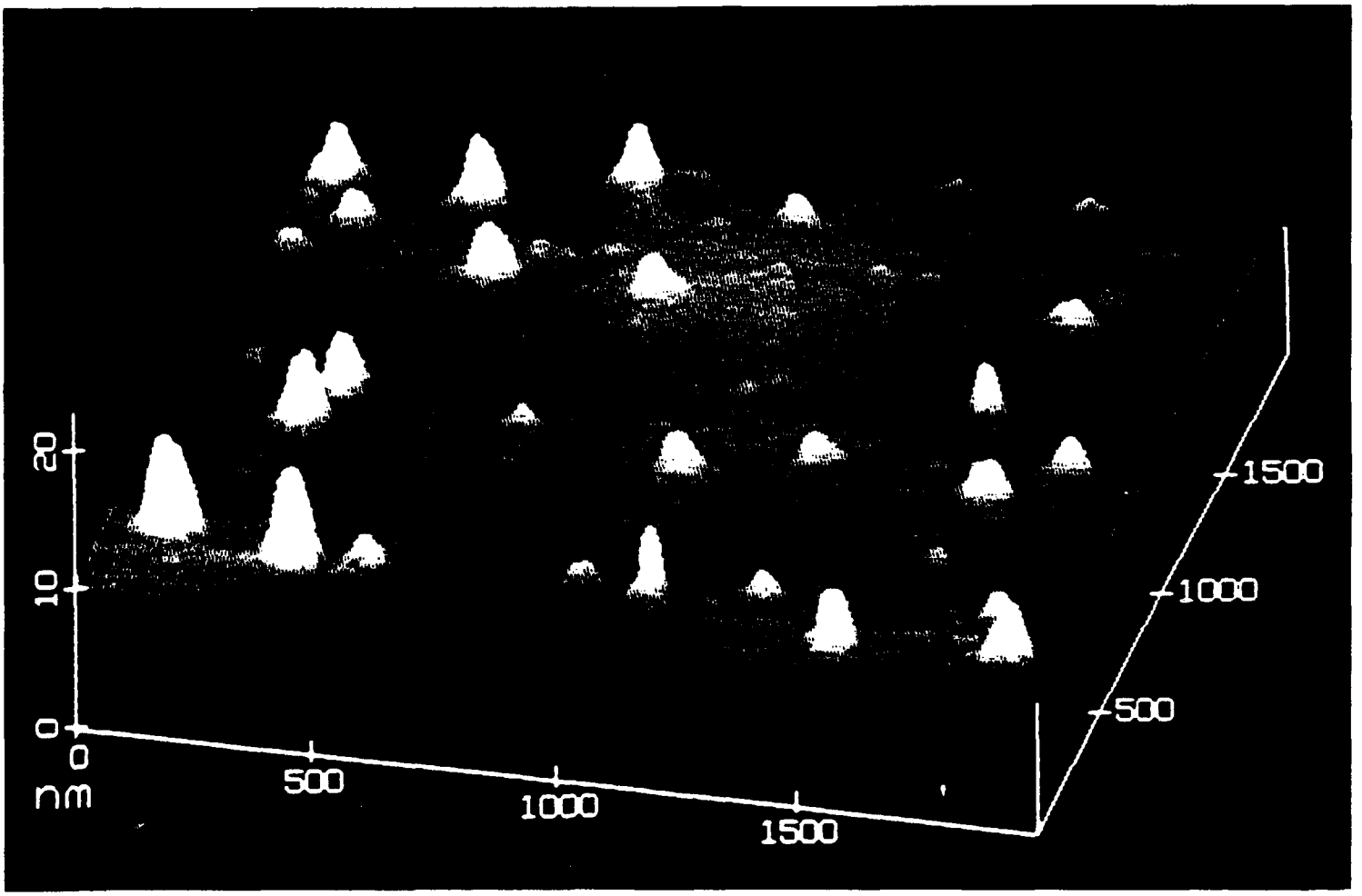

Fig. 6. Three-dimensional AFM image of epitaxial (100) diamond film (sample III) with adsorbed contaminants.

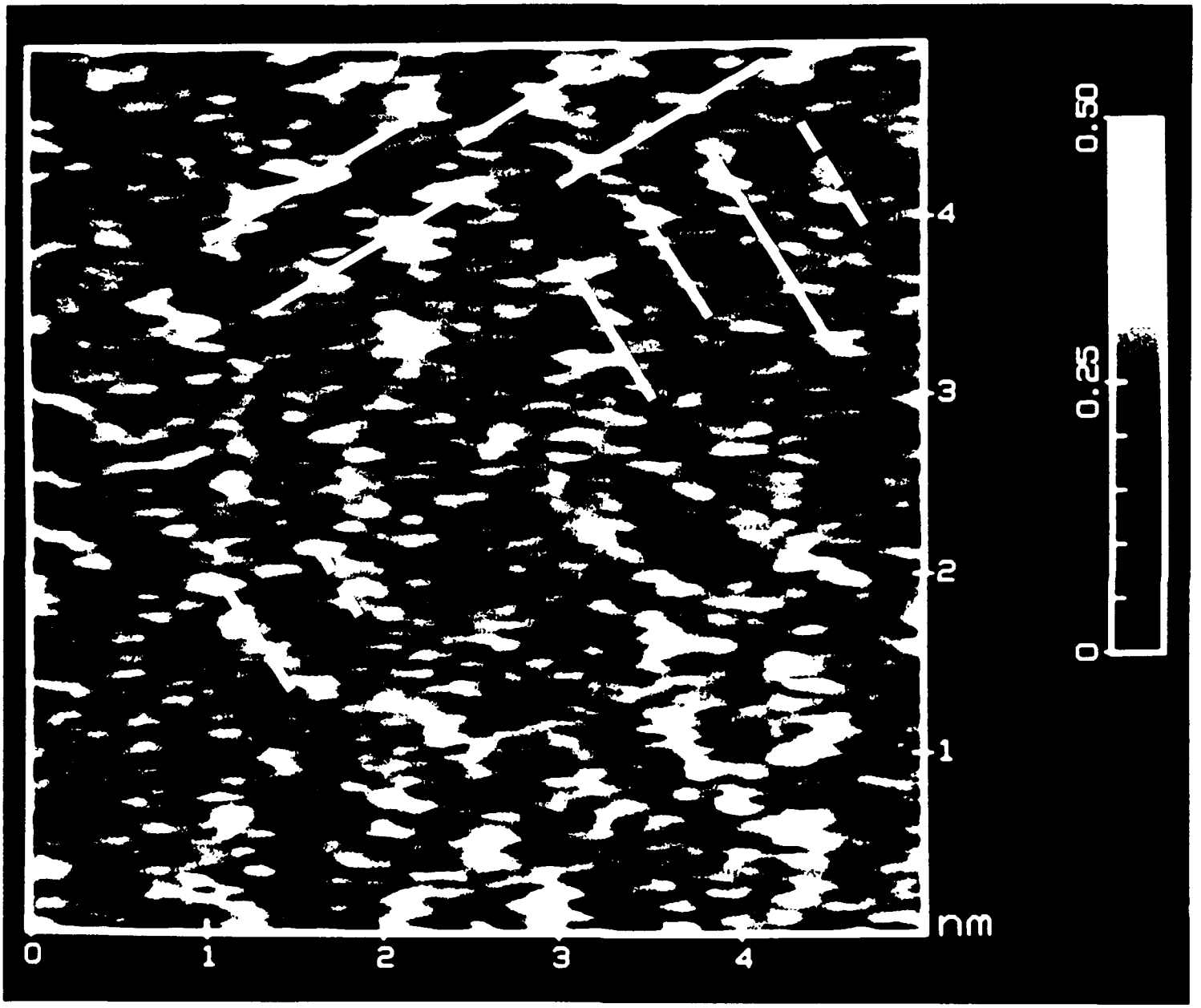

Fig. 7. High-resolution image of epitaxial (100) diamond film (sample III). White traces, separated by 5 Å, represent the location of (2×1) dimer rows.

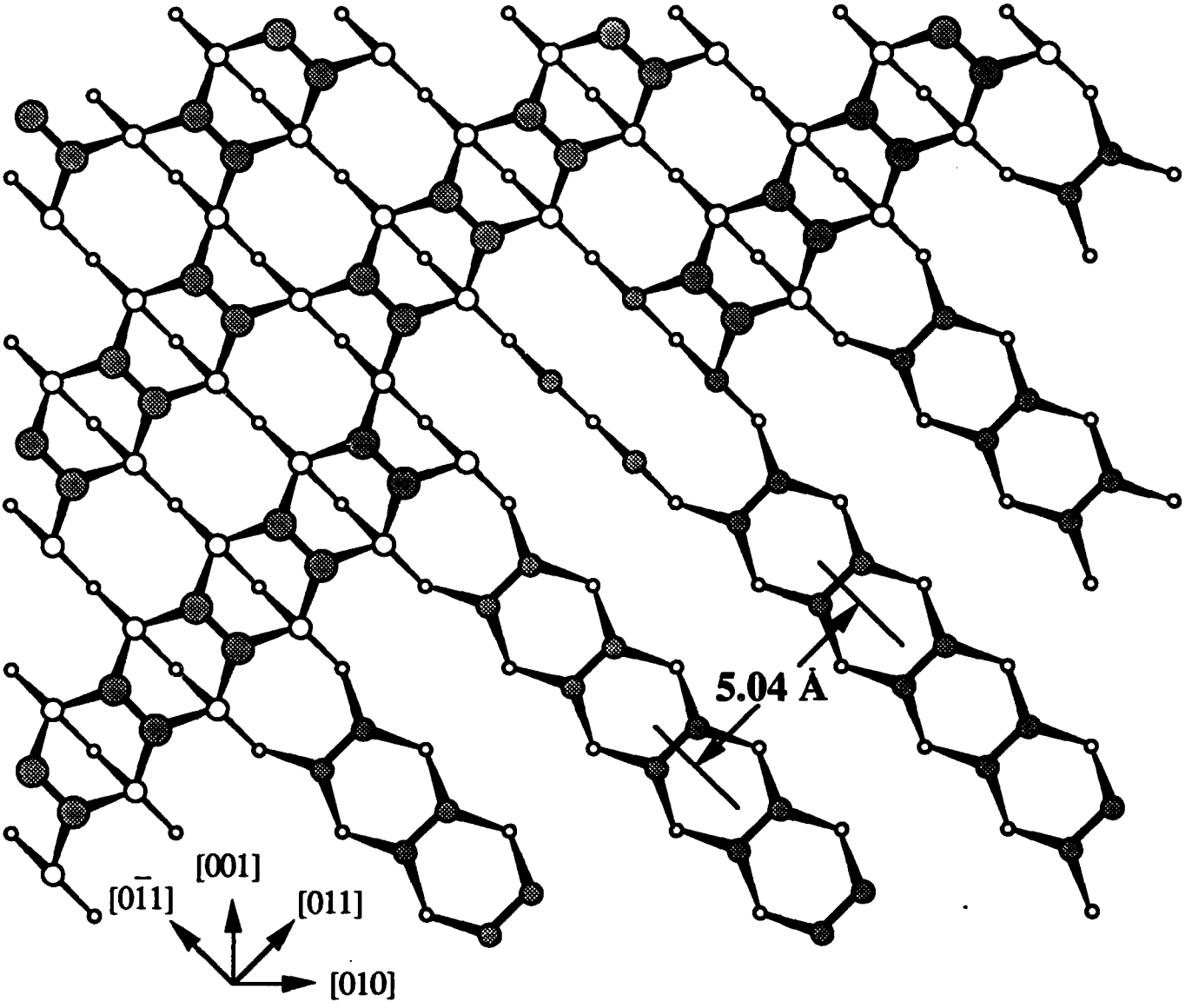

Fig. 8. A top view model surface structure of the AFM image shown in Fig. 7. The shaded circles represent carbon atoms which are also bonded to hydrogen. The diameters of the carbon atoms diminish for each successive layer below the topmost one.

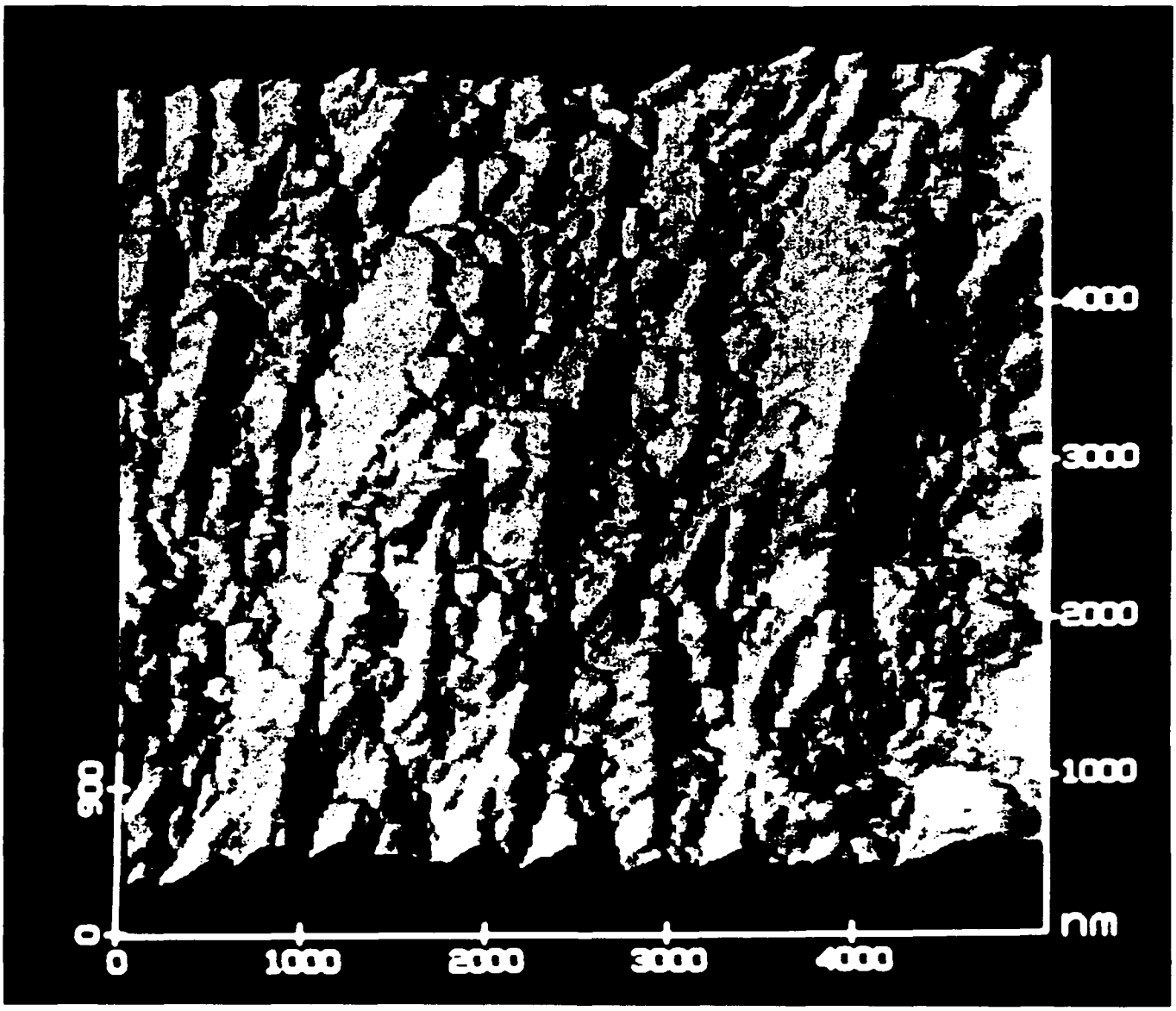

Fig. 9. Three-dimensional view of a representative portion of the (110) film surface (sample IV).

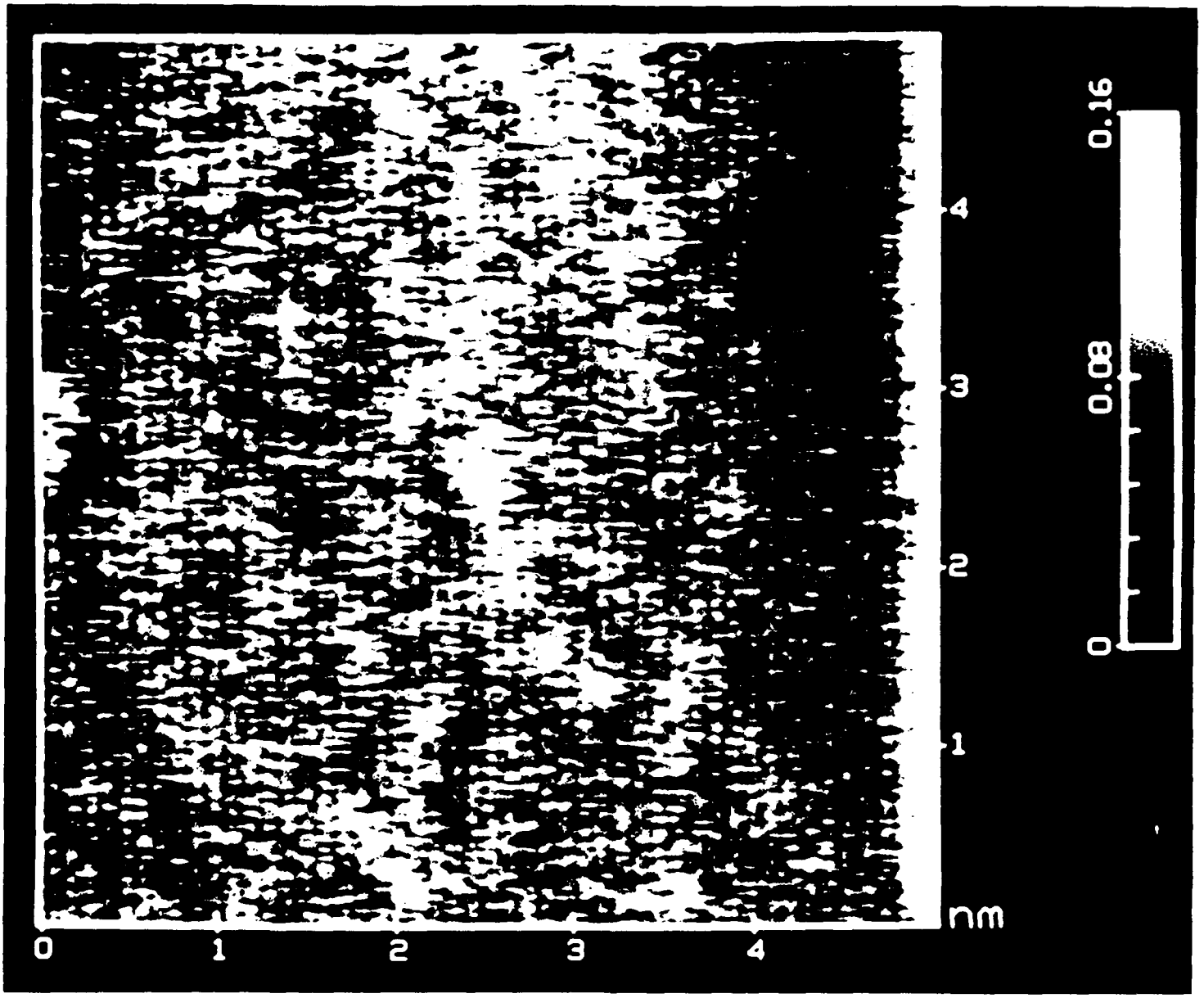

Fig. 10. High-resolution image of the (110) film surface, taken at the top of one of the "hills."

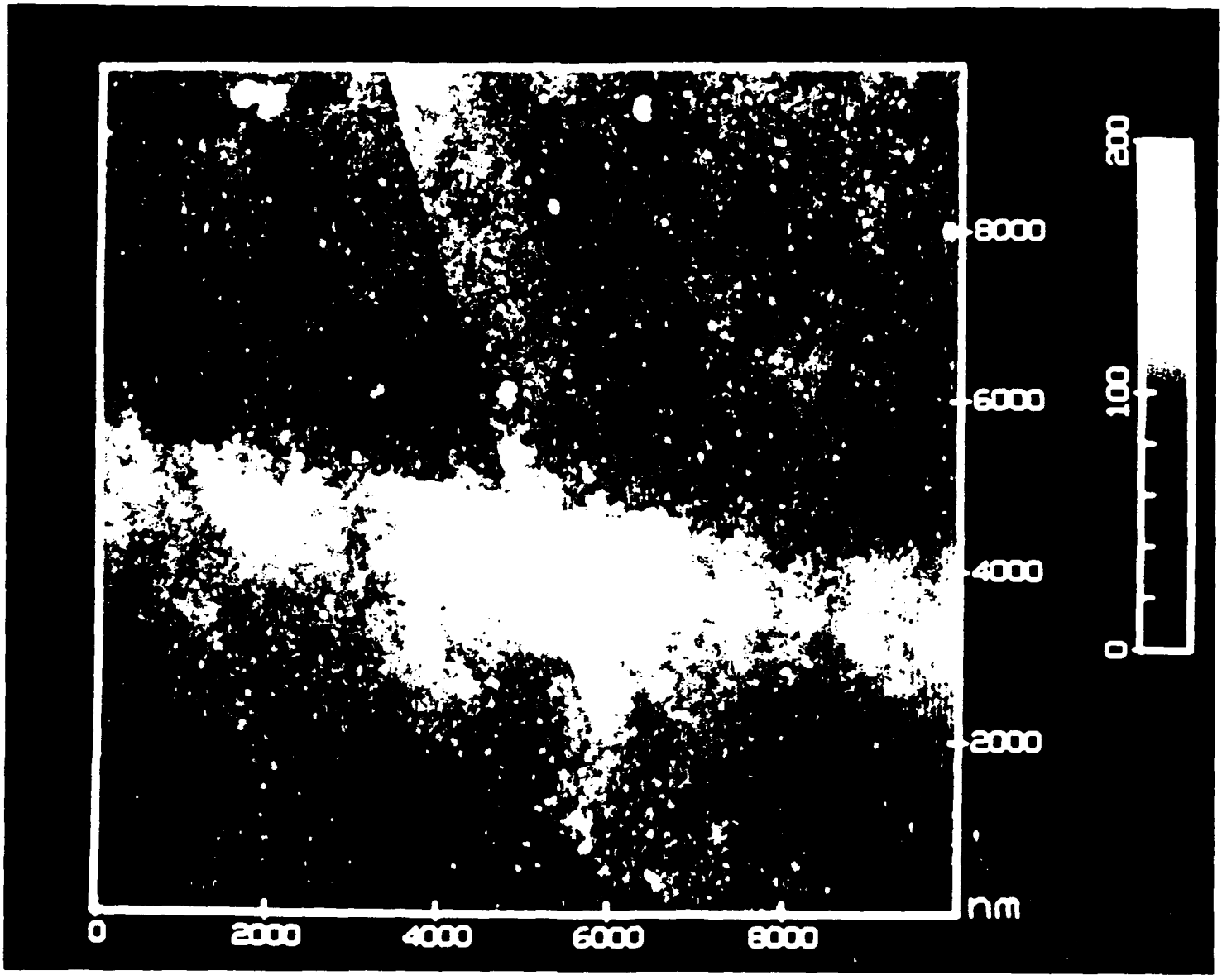

Fig.11. AFM image of the (111) film surface (sample V) showing two intersecting cracks and a locally-rough morphology.